SAI
Conf-[illegible]-0300C

DE82 018809

FRAGMENTATION OF MOLTEN-CORE MATERIAL BY SODIUM*

T. Y. Chu

Sandia National Laboratories**
Albuquerque, New Mexico 87185
U.S.A.

ABSTRACT

A series of scoping experiments was performed to study the fragmentation of prototypic high temperature melts in sodium. The quantity of melt involved was at least one order of magnitude larger than previous experiments. Two modes of contact were used: melt streaming into sodium and sodium into melt.

The average bulk fragment size distribution was found to be in the range of previous data and the average size distribution was found to be insensitive to mode of contact. SEM studies showed that the metal component typically fragmented in the molten phase while the oxide component fragmented in the solid phase. For UO_2-ZrO_2/stainless steel melts no significant spatial separation of the metal and oxide was observed.

The fragment size distribution was stratified vertically in the debris bed in all cases. While the bulk fragment size showed generally consistent trends, the individual experiments were sufficiently different to cause different degrees of stratification in the debris bed. For the highly stratified beds the permeability can decrease by as much as a factor of 20 from the bottom to the top of the bed.

INTRODUCTION

Many severe accident scenarios, either in-vessel or ex-vessel, for advanced sodium-cooled reactor systems lead to the contact between high temperature melt and sodium. The nature of fuel fragment debris resulting from this contact strongly influences the coolability of the settled debris bed and the subsequent probability of remelting as a threat to the containment system. Previous investigations yielding quantitative information involve very small quantities of fuel melt, leaving unanswered the question as to whether or not large quantities would yield different results. Because no analytical scaling laws were available, a series of scoping experiments was performed to clarify this question.

In the present series of experiments, melts of core material about a factor of 10 larger than previously used were contacted with sodium. Two modes of contact were used: melt streaming into sodium (forward experiment) and sodium into melt (reversed experiment). Bulk fragment analyses of the debris size distribution were in general agreement with previous smaller scale studies. In

*This work sponsored by the United States Nuclear Regulatory Commission

**Operated for the United States Department of Energy under contract number DE-AC04-76DP00789

DISCLAIMER

addition, new results were obtained concerning the detailed structure of the debris bed.

DESCRIPTION OF TESTS

The test vessel consists of an inner magnesium oxide vessel, 34 cm in I.D. and 46 cm deep, and a stainless steel jacket. The test vessel is totally enclosed by a taller, outer steel vessel. For forward experiments, the test vessel was filled with 23 kg of sodium (28.5 cm deep at 500°C) and the melt produced by metallothermic reactions was drained into the vessel through a 5.1 cm opening in the head of the outer vessel approximately 70 cm above the sodium level. Details of the test apparatus were presented in reference [1]. For the reversed experiments, the metallothermic reaction is set off in the test vessel and the sodium is released through a 10.2 cm opening approximately 100 cm above the melt level.

A total of five forward experiments and two reversed experiments were performed. In each series, one of the experiments used 14 kg of iron/Al_2O_3 (44 W/O) melt and the other experiments used 20 kg of a stainless steel/UO_2, ZrO_2 (70 W/O) corium-like melt. In all cases the melt temperature was estimated to be at about 2600°C and the sodium temperature varied from 250°C to 690°C. The test conditions of all the tests are summarized in Table I.

Since the focus of the present paper is on the study of the debris bed, only a brief description of the melt coolant interaction will appear here as background. In all the experiments, the interactions were characterized by a series of pressure events typically fairly equally spaced in time. Thermocouple data indicated that the effect of each interaction reached throughout the entire pool. During these events, sodium slugs were sent up against the vessel head. Some of the impacts were sufficient to cause the 1000 kg apparatus to jump approximately 2 cm. The energy involved is an insignificant (of the order of .001%) fraction of the total melt energy.

RESULTS

Bulk Fragment Distribution

After each experiment several core samples of the debris bed were obtained by driving thin walled tubing into the frozen sodium pool. The reaction vessel was then placed on its side and a fine mist spray of water was used to react away the sodium. Both the fragments and the reactant solution were collected in a stainless steel vessel. Ammonium nitrate was added at intervals to neutralize the solution. The reactions were kept at a very slow rate, about 3 mm/hr, to minimize possible disruption to the fragments. Several days were allowed for the particles to settle out.

The fragments from each test were classified by sieving with sieve sizes ranging from 44 μm to 2830 μm. The size distributions are plotted in Figure 1. All the data followed a general trend with 85% to 95% of the fragments less than 2830 μm and one to eight percent of the fragments less than 44 μm. Visual examination of individual fragments from each experiment showed fairly similar appearances for each experiment except for FRAG 6. In this particular experiment the sodium temperature was at 690°C while in other experiments the sodium temperature ranged from 250°C to 509°C. Because of the high temperature of the sodium, the melt stream was able to reach all the way to the bottom of the pool without fragmenting completely and resulted in some fragments of the order of 5 cm. However, even in this case the total quantity of large fragments was still relatively small and the distribution was still substantially the same as from

other experiments. The distributions of all forward and reversed experiments were averaged to obtain a general comparison of the effect of the mode of contact, i.e., melt into sodium versus sodium into melt. Except for a slight divergence for large particle sizes the two sets of averages appeared to be essentially identical as shown in Figure 2 and in the following table:

Table II

Particle Size, μm	2830	1190	840	600	420	210	105	44
Forward %*	93.1	75.1	68.5	58.6	48.3	28.9	15.5	6.4
Reversed %*	88.0	70.6	64.3	55.6	46.8	30.3	16.6	6.1

*Denotes % less than the indicated size.

The fine fragments, less than 44 μm, were further classified by sedimentation. Approximately 85% of the fine fragments had an equivalent spherical diameter of less than 10 μm.

Previous fragmentation studies [1], [2] often involved masses much less than those of the present experiments. The largest and most similar to the present experiments were the M series [2] carried out at ANL. The actual mass fragmented in these experiments was typically one order of magnitude less than the present experiments. However, as Figure 3 shows, the two sets of data are remarkably similar. Therefore, at least up to the range of 10 kg melt fragmentation does not appear to be very scale dependent.

Debris Bed Structure

To obtain a graphical representation of the structure of the bed in the vertical direction core samples of the debris bed were X-rayed with the X-ray beam oriented perpendicular to the axis of the core along two diameters 90° apart. A gamma-ray attenuation technique was used to determine the average density profile of the bed. To characterize the debris bed further, each core was then cut into disks 6.4 to 12.7 mm thick. X-ray photographs were then taken along the axis to obtain a more detailed local display of the bed structure.

Following the nondestructive characterization, the sodium in the core disks was removed. Also the local fragment weight fraction of the core was obtained by weighing each core disk before and after the removal of the sodium. The average density of fragments from each core disk was measured using helium pycnometry. Finally, scanning electron micrographs (SEM) were taken of the fragments.

Typically the bed depth in the present experiments varied from 50 to 75 mm. These variations resulted from mass ejected from the top of the vessel in some of the experiments. Bed density measurements showed a nearly constant density in the lower bed, and above that a zone about 20 to 30 mm thick in which a smooth transition to pure sodium occurs.

Visual inspection of the X-ray (Figure 4) and fragments (Figure 5) of the core samples indicated that the particle size distribution in the debris bed was stratified, as predicted in previous theoretical studies [3]. The particle size

stratification was quantified by classifying the fragments from each core disk. Figure 6 shows a typical result from FRAG 11. The degree of stratification varied from experiment to experiment. The median particle size varied by a factor of 3 to 10 from the bottom to the top of the bed. Because the degree of stratification depends on the fall distance of the particles, it could depend on a number of factors such as the number, location, and intensity of the fragmentation interactions as well as the final pool depth in the experiment. Pool depth was probably a significant influence in the present experiments since the more stratified beds were associated with later experiments where the test fixture was modified to prevent mass ejection during interactions and thus resulted in deeper pools and deeper beds.

Figures 7A and 7B are scanning electron micrographs (SEM) of the fragments. Most of the metal fragments and a small fraction of the oxide fragments appeared to have smooth and nearly spherical surfaces indicating that fragmentation took place while the material was still molten. On the other hand, most of the oxide fragments display angular outlines indicating fragmentation in the solid phase due to stress. This difference is more pronounced for the UO_2-ZrO_2/stainless steel melt than for the Al_2O_3/iron melt because Al_2O_3 has a lower solidification point. In general, relatively few long and slender particles appear to be present. The ratio of dimensions in two perpendicular directions on a cross-section of a fragment on the average is certainly less than two. An examination of the fragments and SEM photographs showed that for UO_2-ZrO_2/stainless steel melt there was no significant separation of the metal and oxide phases. But for FRAG 9 which was a reversed experiment using Al_2O_3/iron melt there appeared to be less iron in the upper region of the bed as compared to the bottom region of the bed, Figure 7A. From local density data assuming fully dense fragments, the bottom of the bed was calculated to be 50% iron by volume and the top of the bed should have 23% iron by volume. These values seem to be in agreement with the SEM photographs. The difference in metal oxide separation for the two melts is probably mainly due to the much larger relative density difference in the Al_2O_3/iron melt.

For quantitative evaluation of the coolability of a debris bed a knowledge of the void fraction of the bed is desired. This information together with particle size distribution can be used to calculate the permeability of the bed. The void fraction, ε, of the debris bed can be calculated using the relation

$$\varepsilon = (1-WF)\,\frac{\overline{\rho}}{\rho_s}$$

where WF is the weight fraction of the fragments and $\overline{\rho}$ and ρ_s are the average density of the bed and density of sodium respectively. The value of ρ can be obtained from gamma-ray attenuation measurements. However, in experiments involving melts containing UO_2, the technique is not particularly accurate because the attenuation coefficient for UO_2 is much higher than the other melt components and sodium. Furthermore, because the beam is of comparable size to large fragments, large spatial fluctuations result in the average density measurements. Instead, the average bed density was calculated from fragment average density, ρ_F, from each core section (typically 12.7 mm thick):

$$\overline{\rho} = \frac{\rho_F \rho_s}{(1-WF)\rho_F + W_F \rho_s}$$

Using this method the void fraction of four experiments was calculated (see Figure 7; the location of the bar is the top of the bed as indicated by X-ray photographs). The void fraction of the bed is fairly constant near the bottom of the bed; a smooth transition to pure sodium (100% void fraction) took place in the top 20 to 30 mm of the bed. The nearly constant void fraction in the bed is a direct consequence of the similarity of the fragment size distributions in the bed, see Figure 5. If each distribution was normalized by its median value then all the distributions would be reduced to a single line.

To evaluate permeability variations, an effective spherical diameter defined as

$$d_{eff} = \frac{1}{\Sigma(\frac{W_i}{d_i})}$$

is used where W_i denotes the weight fraction of particles with a diameter d_i. In the present experiments, a total of six cuts were made of the fragments. Figures 9A and 9B depict two typical variations of d_{eff} as a function of bed depth. In each case, location 1 is in the center of the bed and other locations are 15 cm away from the center. As Figures 9A and 9B show, and in general, the beds formed in the reversed experiments were much less uniform horizontally than the beds for the forward experiments. This is mainly the result of the difference in experimental configurations. In the reversed experiments steel and oxide separated due to density differences and because of the large horizontal dimension occupied by the melt, the steel in the melt tends to collect to one side of the vessel rather than forming a uniform layer. While individual size and bed depth may be different from location to location, stratification was always observed.

Local permeability, P, for the debris bed can be estimated from the void fraction and fragment size distribution data using the Black-Kozeny model [4]:

$$P = \frac{\varepsilon^3}{C(1-\varepsilon)^2} d_{eff}^2$$

where C is a constant. Figure 10 shows typical results. In presenting the results, the permeability at each depth was normalized by the permeability at the bottom of the bed. The permeability was found to decrease most significantly near the top of the bed owing to size stratification. For the most stratified bed, FRAG 11, the bed permeability decreased by a factor of 20 near the top of the bed. This variation could have a profound influence on the coolability of the debris bed.

SUMMARY AND DISCUSSION

A series of scoping experiments was performed to study the fragmentation of prototypic high temperature melts in sodium. The quantity of melt involved was at least one order of magnitude larger than previous experiments. The average bulk fragment size distribution was found to be in the range of previous data and the average size distribution was found to be insensitive to the mode of contact. SEM studies showed that the metal component typically fragmented in the molten phase while the oxide component fragmented in the solid phase. For UO_2-ZrO_2/-stainless steel melts no significant spatial separation of the metal and oxide were observed while Al_2O_3/iron melts did exhibit spatial separation of metal and oxide. The separation observed can be attributed to relatively large differences in densities of the two components.

The fragment size distribution was stratified vertically in the debris bed in all cases. In the reversed experiments the horizontal distribution of fragments were also highly nonuniform but this was the result of the configuration of the initial melt pool. While the bulk fragment size showed generally consistent trends, the individual experiments were sufficiently different to cause different degrees of stratification in the debris bed. For the highly stratified beds the permeability can decrease by as much as a factor of 20 from the bottom to the top of the bed.

The geometry in the present experiments is not prototypic; therefore, the quantitative data of the debris bed are not directly applicable to reactor accident assessment. However, the general qualitative observations are all relevant to post-accident heat removal studies. In fact, because of the larger scale of a prototypical accident, the effect of fragment size stratification is likely to be even more pronounced.

REFERENCES

1. Mizuta, H., "Fragmentation of Uranium Dioxide after Molten Uranium Dioxide-Sodium Interaction," Journal of Nuclear Science and Technology, 11 [11], pp 480-487, November 1974.

2. Sowa, E. S., et al., "Molten Core Debris-Sodium Interactions: M-Series Experiments," Proceedings of the International Meeting on Fast Reactor Safety Technology, Seattle, Washington, August 19-23, 1979, pp 733-741.

3. Rivard, J. B. and R. L. Coats, "Post-Accident Heat Removal: An Overview of Some In-Vessel Safety Considerations," Proceedings of the International Meeting on Fast Reactor Safety Technology, Seattle, Washington, August 19-23, 1979, pp 709-720.

4. Bird, R. B., W. E. Stewart and E. N. Lightfoot, Transport Phenomena, John Wiley & Sons, New York, p 200.

Table I Experimental Conditions for Forward and Reversed Experiments

	Forward: Melt into Sodium					Reversed: Sodium into Melt	
	FRAG 2	FRAG 4	FRAG 5	FRAG 6	FRAG 13	FRAG 9	FRAG 11
Steam Size (mm)	51	51	51	51	51	102	102
Melt	Fe Al_2O_3 (44%)	UO_2-ZrO_2 (70%) stainless steel	UO_2-ZrO_2 (70%) stainless steel	UO_2-ZrO_2 (70%) stainless steel	UO_2-ZrO_2 (70%) stainless steel	Fe Al_2O_3 (44%) steel	UO_2-ZrO_2 (70%) stainless
Melt Mass (kg)	13	20	20	20	20	14	20
Sodium (kg)	23	23	23	23	23	23	23
Sodium Temperature (^{o}C)	480	420	250	690	500	500	509
Material Recovered from Interaction Vessel*	7.0	12.9	15.0	11.2	7.0	11.4	14.2

* Material recovered outside of the vessel was not classified.

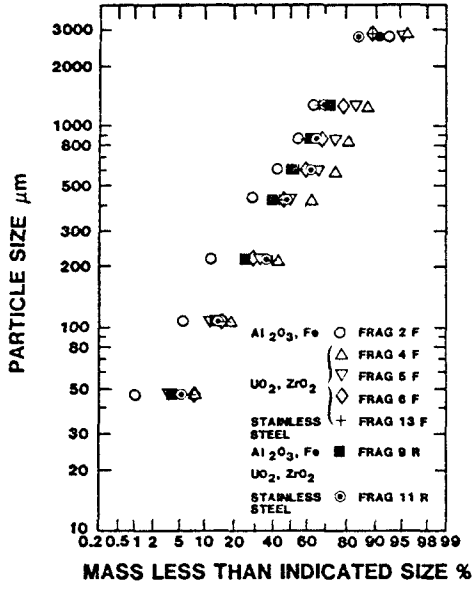

Figure 1. Bulk Fragment Size Distributions

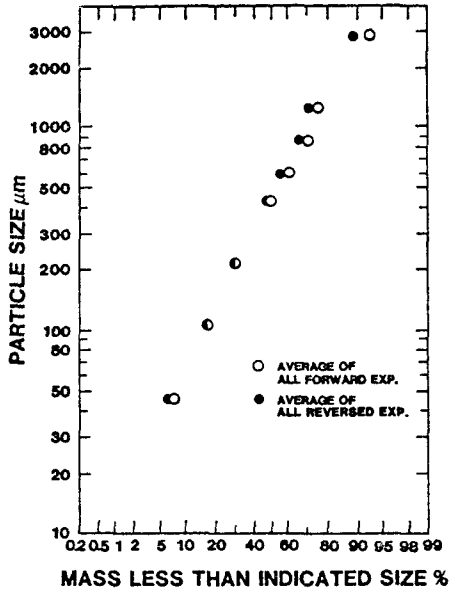

Figure 2. Comparison of Averaged Particle Size Distribution for Forward and Reversed Experiments

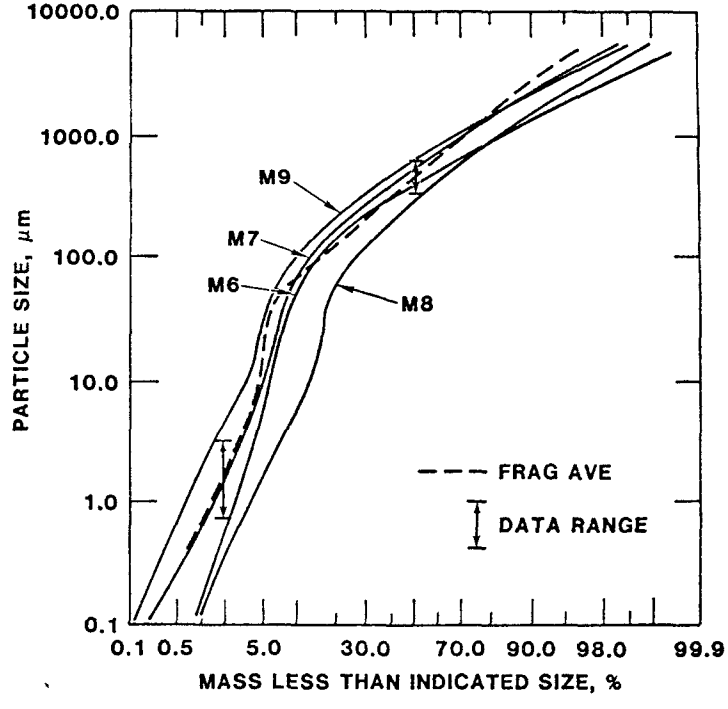

Figure 3. Comparison of Bulk Fragment Distribution with M-Series Experiments [2]

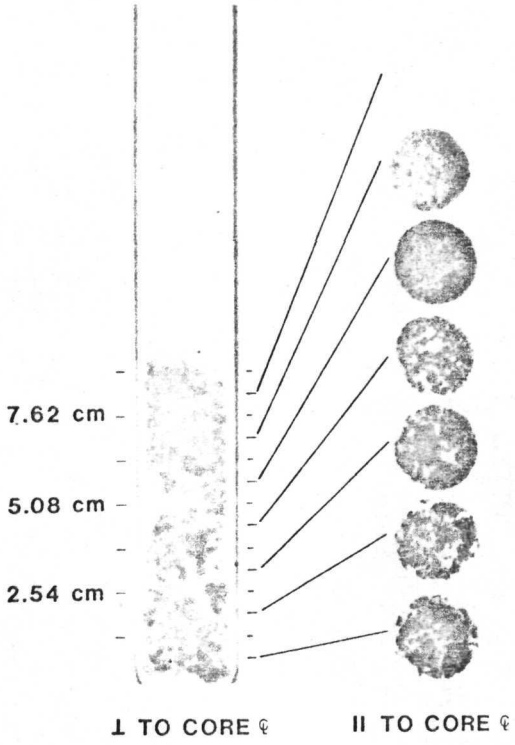

Figure 4. X-Ray of Debris Bed, Frag 11

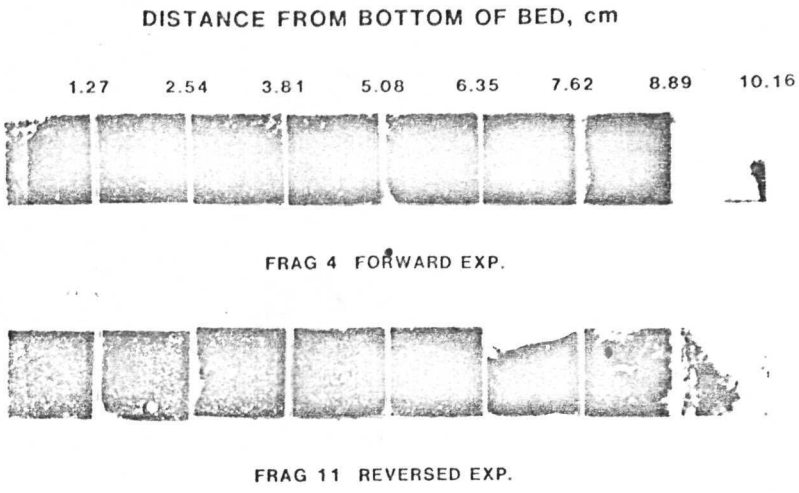

Figure 5. Fragment from Different Depth of the Debris Bed (Both Cores from Bed Center)

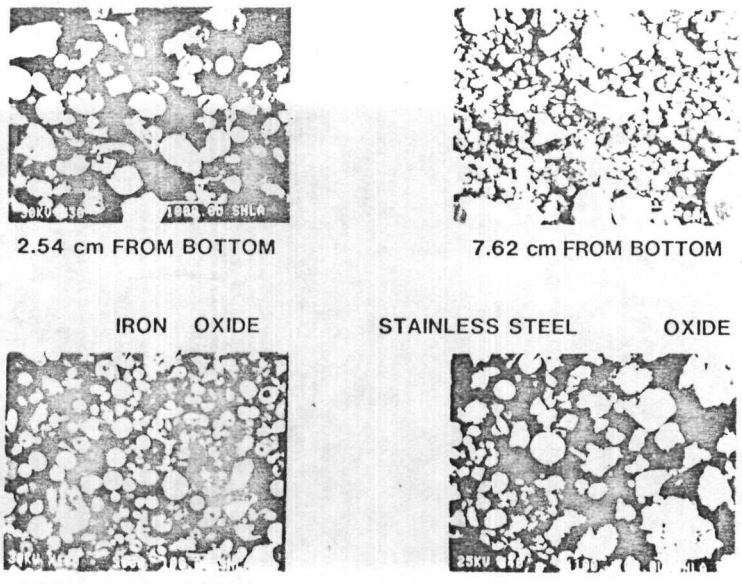

Figure 7. SEM of Debris for FRAG 9 and FRAG 11

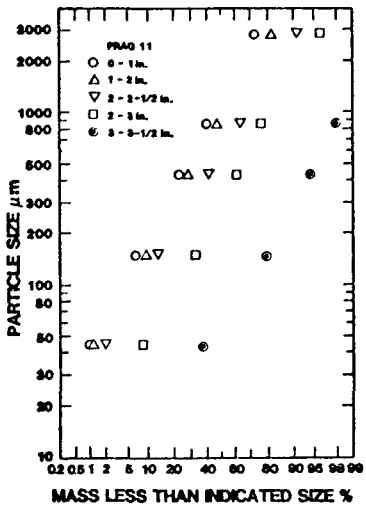

Figure 6 Layer by Layer Particle Distribution from the Center of the Bed (Core Sample No 1)

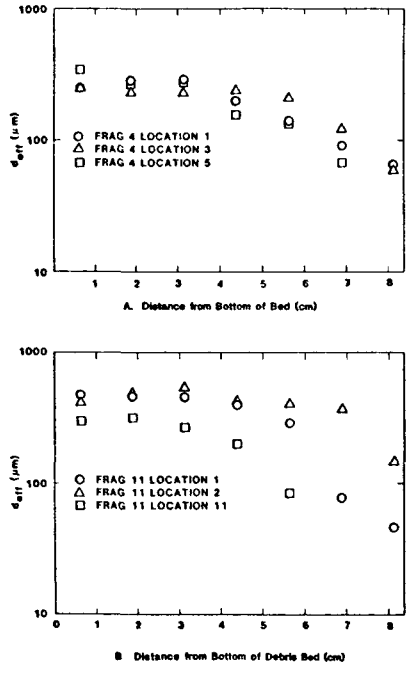

Figure 9 Two Variations of Effective Spherical Diameter

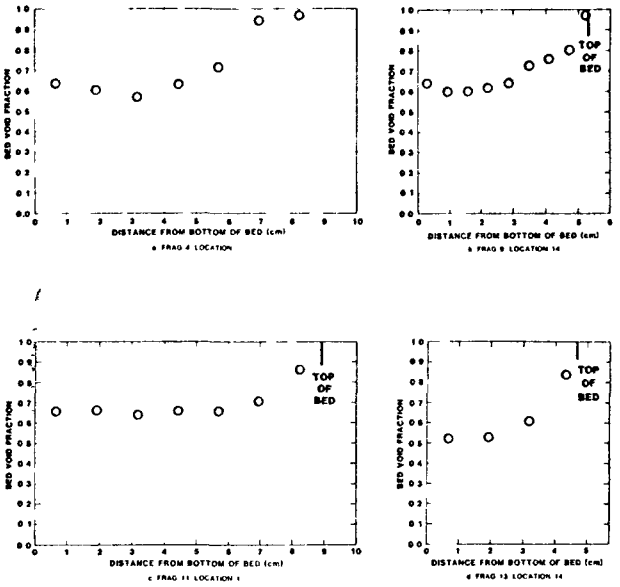

Figure 8 Calculated Void Fractions for 4 Experiments

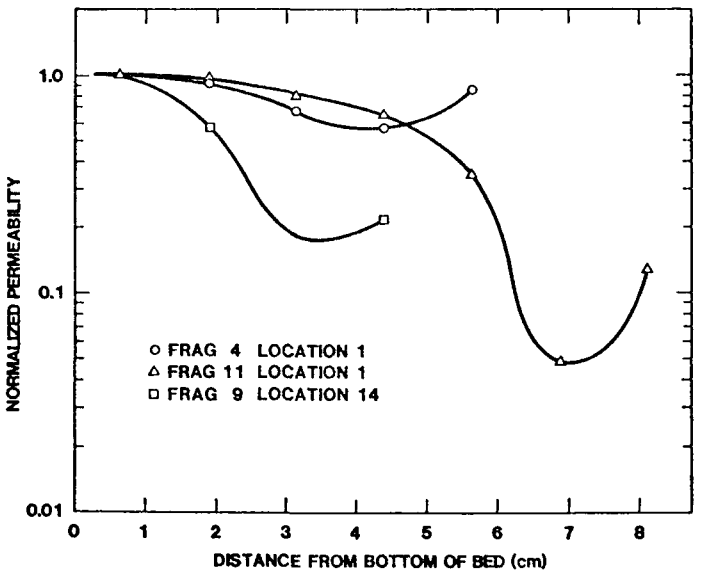

Figure 10 Permeability vs Bed Depth